Coordination Chemistry Reviews 254 (2010) 1803–1811

Contents lists available at ScienceDirect

Coordination Chemistry Reviews

journal homepage: www.elsevier.com/locate/ccr

Review

Electronic structures, photophysical properties, and electrochemistry of ruthenium(II)$(bpy)_2$ pyridylimidazole complexes

Kyle M. Lancaster[a], James B. Gerken[b], Alec C. Durrell[a], Joshua H. Palmer[a], Harry B. Gray[a,*]

[a] Beckman Institute, California Institute of Technology, 1200 E California Blvd, Pasadena, CA 91125, USA
[b] Department of Chemistry, University of Wisconsin-Madison, Madison, WI 53706, USA

Contents

ARTICLE INFO

Article history:
Received 20 August 2009
Accepted 9 April 2010
Available online 24 April 2010

Keywords:
Ruthenium
Pyridylimidazoles
Photophysics
Cyclic voltammetry

ABSTRACT

The properties of Ru^{II} complexes involving the imidazole moiety are discussed. Complexes $[Ru(bpy)_2(L)]^{2+}$ [bpy = 2,2′-bipyridine, L = 2-(2′-pyridyl)imidazole (2-pimH) and 4-(2′-pyridyl)imidazole (4-pimH)] have been synthesized and fully characterized. Reduction potentials are 0.76 V vs. Fc^+/Fc^0 for both complexes in acetonitrile solution, and the deprotonated complexes undergo irreversible electrochemical oxidation at 0.38 V vs. Fc^+/Fc^0. Density functional theory (DFT) calculations suggest that oxidation of the protonated complexes is primarily metal-based and that of the deprotonated complexes is ligand-centered. The pK_a of the 4-pimH complex was found to be 9.7 ± 0.2; the pK_a of the 2-pimH complex is 7.9 ± 0.2. Luminescence lifetimes (L = 4-pimH, 277 ns; 2-pimH, 224 ns; $4pim^-$, 40 ns; $2pim^-$, 34 ns in 5% methanol/water solution) combined with quantum yield data and acid–base behavior suggest that the non-coordinated imidazole nitrogen tunes deactivation pathways.

1. Introduction

The complexes of ruthenium with bidentate, L_2-type heteroaromatic ligands exhibit rich photochemistry arising mainly from excited state electron-transfer reactions [1–5]. Among the panoply of such ligands, pyridylimidazoles are of interest because complexes of the two isomers, 4-(2′-pyridyl)-imidazole (4-pimH) and 2-(2′-pyridyl)-imidazole (2-pimH) (Fig. 1) should allow further investigation and discussion of the effects of subtle differences in structure on the chemical properties of this molecular family. Moreover, the presence of non-coordinated, ionizable amines opens avenues of investigation into excited state acid–base behavior and proton-coupled electron transfer (PCET).

PimH isomeric differences were first described by Holmes et al. in a series of papers on association constant measurements and calorimetry of the reactions of 2-pimH and 4-pimH with various first-row transition elements [6–8]. These observations showed a general trend of weaker binding by 2-pimH than 4-pimH, with both being less strongly binding than bpy, a trend attributed to decreasing π-acceptor strength [7]. Holmes et al. [9] and Lions et al. [10] also noted an increase in the acidity of the pimH amine proton on complexation to metals, but did not quantify the change in pK_a.

* Corresponding author.
E-mail address: hbgray@caltech.edu (H.B. Gray).

0010-8545/$ – see front matter © 2010 Published by Elsevier B.V.
doi:10.1016/j.ccr.2010.04.005

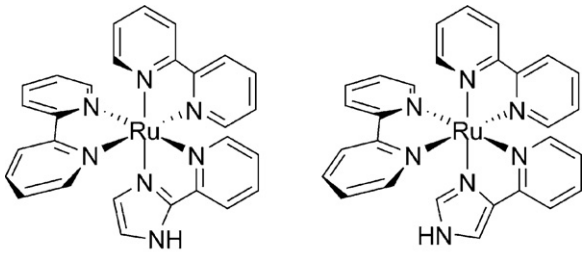

1 2

Fig. 1. Structures of $Ru(bpy)_2$ 2-pimH (**1**) and 4-pimH (**2**) complexes.

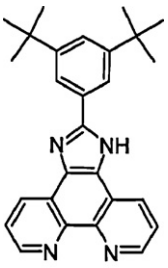

3

Fig. 2. Structure of 2-(3,5-di-*tert*-butylphenyl)imidazo[4,5-*f*]-[1,10]-phenanthroline.

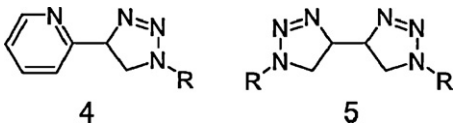

4 5

Fig. 3. Structures of 2′-(1,2,3-triazol-4-yl)pyridine (**3**) and 4,4′-bis(triazole) (**4**).

Later, Boggess and Martin reported a pK_a range of 8–10 for various $[M(2\text{-pimH})_3]^{2+}$ complexes and 13.4 for the free ligand [11]. Herein, we review the literature on Ru-pimH complexes with an emphasis on their photophysics and electrochemistry, and report an extension of Haga's work [12,13] on $[Ru(bpy)_2(2\text{-pimH})]^{2+}$ (**1**) including comparison to the heretofore unreported $[Ru(bpy)_2(4\text{-pimH})]^{2+}$ (**2**).

2. Properties of Ru^{II} complexes with pyridylimidazole and related ligands

Ru(II) complexes of 2-pimH, for which facile ligand syntheses exist, have been more extensively studied than those of 4-pimH. An enantiomerically enriched material was produced by synthesizing the homoleptic complex $[Ru(2\text{-pimH})_3]^{2+}$ [14–17] in the presence of (+)tartrate; its circular dichroism spectrum is similar to that of resolved $[Ru(bpy)_3]^{2+}$ aside from a change in sign indicative of either a reversed Cotton effect or a shift from Δ to Λ as the favored enantiomer [14]. Cooling $[Ru(2\text{-pimH})_3]^{2+}$ to 77 K revealed photoluminescence; Braun et al. attributed its absence at room temperature to rapid ^{3}MLCT (metal to ligand charge transfer) to ^{3}MC (metal-centered) relaxation [15]. Braun observed the $Ru^{III/II}$ couple, however, no electrochemical reduction of $[Ru(2\text{-pimH})_3]^{2+}$ is observable in acetonitrile, which speaks to the high-lying LUMO of the complex [15]. A cathodic shift of the $Ru^{III/II}$ couple by 0.92 V was observed on full deprotonation of this complex [17]. Comparison of this shift with the 0.38 V cathodic shift observed by Haga on deprotonation of $[Ru(bpy)_2(2\text{-pimH})]^{2+}$ led the investigators to conclude that the stabilization of the higher oxidation state in the deprotonated homoleptic complex is mostly of electrostatic origin.

A detailed experimental and theoretical investigation has been reported on the effects of protonation states of a distal, non-coordinated imidazole motif on the electrochemistry and photophysics of $Ru(bpy)_2$(PhenImHPh) [PhenImHPh = 2-(3,5-di-*tert*-butylphenyl)imidazo[4,5-*f*]-[1,10]phenanthroline (**3**), Fig. 2] [18]. The investigators indicate that though the imidazole nitrogen atoms are not directly coordinated to the ruthenium, their protonation states dramatically perturb the excited state lifetimes of the molecule. Moreover, acid–base behavior allowed assignment of excited state localization to either the bpy or PhenImHPh ligands that was supported by theoretical results.

The isomeric complex $[Ru(tpy)(bpy)imidazole]^{2+}$ and some derivatives have been prepared [19]; their reported photophysical properties have not been extensively interpreted but are broadly similar to **1** and **2** (*vide infra*) with differences due to the more extensively conjugated terpyridine ligand. Other monopyridylimidazole Ru complexes have been prepared with η^5-cyclopentadienyl and phosphine [20], η^6-benzene and chloride [21], and bis(β-diketonato) [22] ligands. The $[Ru(2\text{-pimH})(\beta\text{-diketonato})_2]$ complexes display rich hydrogen atom transfer (HAT) chemistry at the free imidazole nitrogen that depends on the electronic nature of the ancillary ligands [22]. The general trends are as expected, with the more electron-withdrawing β-diketonate raising the MLCT energy, oxidation potential, and N–H bond dissociation energy (BDE) of the complex while lowering its pK_a.

The absorption spectra and reduction potentials of $[RuL_3]^{2+}$ complexes featuring 2′-(1,2,3-triazol-4-yl)pyridine (**4**) and 4,4′-bis(triazole) (**5**) ligands (Fig. 3) have recently been reported [23]. The MLCT absorption energies of each complex correlate well with the separation of their first anodic and cathodic reduction potentials; this provides experimental corroboration of the electronic structural picture adopted for Ru polypyridine complexes possessing a largely metal-based HOMO beneath low-lying unoccupied ligand orbitals. Similarly, the properties of $Ru(bpy)_{3-x}L_x^{2+}$ (*vide supra*) (x = 0–3) complexes show systematic shifts as the bpy ligands are replaced with less donating 2,2′-bipyrazine and 2,2′-bipyrimidine ligands [24]. The $d\pi \rightarrow \pi^*$ absorptions undergo bathochromic shifting with increasing number of bpy ligands, behavior that is correlated with a decrease in $Ru^{III/II}$ potentials. The optimization of a ruthenium bis-(methylbenzimidazole)pyridine complex for surface-tethered electrocatalytic water oxidation is an elegant demonstration of the application of redox tuning via ligand selection [25].

Despite the electronic tunability afforded by triazole, bipyrimidine, and bipyrazine, this set of ligands has the deficiency of being very weak bases at the distal nitrogen, as is exemplified by the pK_a values of 0.0 and 2.5 for the corresponding $[Ru(NH_3)_5(C_4H_4N_2)]^{3+}$ complexes [26,27]. $[Ru(bpy)_2(bpm)]^{2+}$ and $[Ru(bpy_2)(bpz)]^{2+}$ show excited state pK_a shifts indicative of MLCT states involving the bipyrimidine or bipyrazine [24]; however, sequential protonation of ruthenium bipyrazine complexes requires strongly acidic conditions (>50% H_2SO_4) and leads to quenching of the luminescence [28]. In contrast, free imidazole has a pK_a of 14.2 [29] and its metal complexes are more acidic [30], leading to proton transfers under mild conditions. A similar shift has been observed in 2-pimH complexes [9–11].

Consequently, ruthenium complexes of pimH are of interest as they can undergo both acid–base and redox chemistry, (PCET) [31–33] and other hydrogen-bonding mediated interactions *via* the distal imidazole nitrogen. For example, the HAT kinetics of $Ru^{II}(acac)_2(2\text{-pimH})$ have recently been reported [34]. Intriguingly, the self-exchange reaction shows a k_H/k_D of only 1.5 despite a much higher kinetic isotope effect (KIE) of 23 in the reaction with 2,2,6,6-tetramethyl-piperidine-1-oxyl (TEMPO). If the proton source is a hydroxyl rather than an imidazole ligand, as is the case

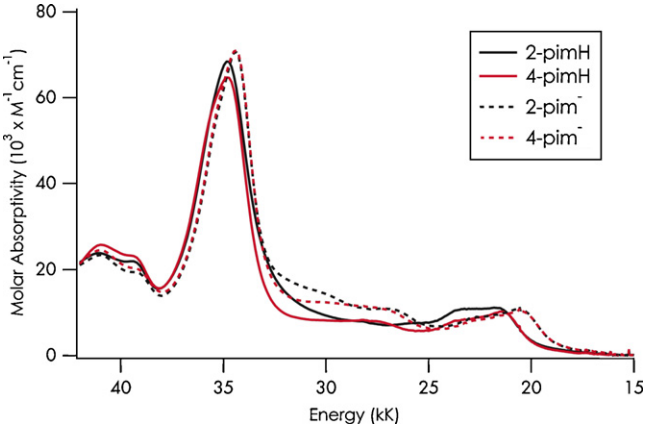

Fig. 4. Absorption spectra of $[Ru(bpy)_2(L)]^{2+}$ and $[Ru(bpy)_2(L–H^+)]^+$ in 5% $MeOH/H_2O$ solution at room temperature.

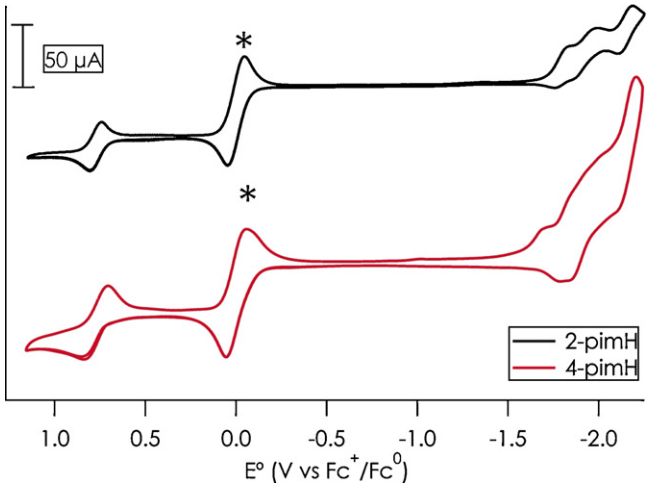

Fig. 5. CVs of 1.5 mM $[Ru(bpy)_2(L)]^{2+}$ in acetonitrile solution at room temperature. Scan rate is 0.1 V/s. Ferrocene was added to sample solutions as an internal standard (Fc^+/Fc^0 wave indicated by an asterisk).

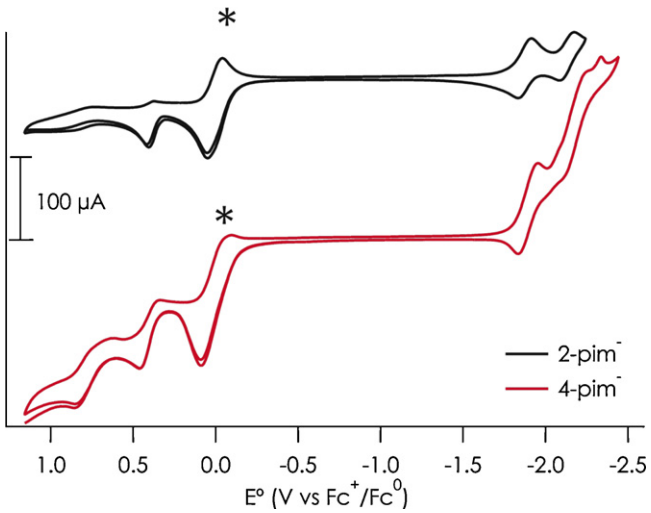

Fig. 6. CVs of 1.5 mM $[Ru(bpy)_2(L^-)]^+$ in acetonitrile solution at room temperature. Deprotonated complexes were generated *in situ* by dropwise addition of concentrated sodium methoxide solution. Scan rate is 0.1 V/s. Ferrocene was added to sample solutions as an internal standard (Fc^+/Fc^0 wave indicated by an asterisk).

for $[Ru^{III}(bpy)_2(py)OH]^{2+}$, the self-exchange rate is similar, and also has a small KIE [35]. This suggests that the imidazole N–H bond in the 2-pimH system behaves similarly to a hydroxyl ligand in some respects. The UV–vis spectrum and electrochemistry of **1** are also sensitive to added heterocyclic bases, with the shifts attributed to hydrogen bonding [13], although PCET could reasonably explain the data. Although pyridyl–benzimidazole complexes are beyond the *sensu stricto* scope of this work, very interesting reactions between the excited state of $[Ru^{II}(bpy)_2(2\text{-pbim}^-)]^+$ (2-pbim$^-$ = 2-(2-pyridyl)benzimidazolate) and quinols with $k_D > k_H$ have been reported [36]. These observations have been explained in the context of PCET theory as arising from coupling of the electronic and proton vibrational states leading to nonadiabatic reactions [37]. In the case of $Ru(bpy)_2$(PhenImHPh), with both imidazole nitrogen atoms available for protonation and hence three protonation states possible, electron transfer in the mono- and depronated states is primarily from the extensively conjugated imidazole-bearing ligand [18].

Despite the abundance of studies involving 2-pimH, there is almost no discussion of 4-pimH, particularly with respect to photophysics and PCET. We attribute this absence to relative synthetic accessibility (the 2-pimH ligand is readily synthesized *via* a modification of the procedure of Radziszewski [38,39]). While many routes to the acquisition of the 4-pimH ligand have been developed since its initial synthesis [40], we chose to modify the method of Wang and Schwabacher [41] in order to more easily isolate the ligand as the dihydrochloride salt. Pyridylimidazoles in hand, ligand exchange with $Ru(bpy)_2Cl_2$ [42] to form **1** and **2** was accomplished using methods typical for $[Ru(bpy)_2L]^{2+}$ complexes, with isolation effected by precipitation of the PF_6^- salts.

3. Absorption spectra

Spectra of $Ru(bpy)_2(L)$ (L = 2-pimH, 4-pimH) were recorded in dichloromethane (Fig. 3, Table 1) and 5% methanol/water (Fig. 4) solutions. The lowest energy band of **2**, attributable to MLCT, is slightly (~0.15 kK) red shifted relative to that of **1**. A more substantial difference in both energy and intensity is exhibited in the next higher-energy MLCT band (23.47, **1**; 23.70 kK, **2**). Interestingly, these ~20 kK MLCT systems appear to merge upon deprotonation of the complexes, suggesting that either the deprotonated pyridylimidazoles are isoelectronic donors, or that ligand energy levels are reordered such that these low-lying MLCT systems become largely bipyridyl-based. Scant changes are observed upon transfer of the complexes to a nonpolar solvent.

4. Redox properties

Cyclic voltammograms (CVs) for **1** and **2** were recorded in acetonitrile solution (Fig. 5). Each complex displays one reversible wave at 0.76 V vs. Fc^+/Fc^0, corresponding to the $Ru^{III/II}$ redox couple. Separation between the anodic and cathodic current peaks for this process is similar (~0.08 V) to that of the Fc^+/Fc^0 wave, supporting the assignment of this feature to a one-electron redox process. Two waves observed at highly negative potentials are attributable to ligand-centered reduction and are analogous to the behavior observed for $[Ru(bpy)_3]^{2+}$ [24]. Precise assignment of the redox loci are not straightforward as in the case of $[Ru(bpy)_2(bpx)]^2$ (bpx = 2,2′-bipyridmidine, 2,2′-bipyrazine).

A concentrated solution of sodium methoxide was added dropwise to electrolyte-containing acetonitrile solutions of each complex with CVs recorded between additions (Fig. 6). Disappearance of the $Ru^{III/II}$ couple in the protonated complexes tracks with appearance of a new, irreversible oxidation wave cathodically shifted to 0.38 V vs. Fc^+/Fc^0. The electrochemical behavior as well as the results of our DFT calculations (*vide infra*) indicate that this new

Table 1
Electronic absorption[a] features of $Ru(bpy)_2(L)^{2+}$.

L	5% MeOH/H_2O pH 3 ν_{max} ($\varepsilon \times 10^{-3}$ M^{-1} cm^{-1})	5% MeOH/H_2O pH 12 ν_{max} ($\varepsilon \times 10^{-3}$ M^{-1} cm^{-1})	Dichloromethane ν_{max} ($\varepsilon \times 10^{-3}$ M^{-1} cm^{-1})
(2-pimH)	23.47 (10.5), 21.51 (11.0)	22.83 (8.00), 20.49 (10.70)	23.47 (10.60), 21.51 (12.10)
(4-pimH)	27.40 (8.30), 23.70 (7.80), 21.37 (10.20)	26.88 (9.80), 22.94 (7.00), 20.41 (10.20)	27.40 (8.80), 23.53 (8.00), 21.37 (10.90)

[a] Absorption energies are reported in kilokaisers. Uncertainties in band positions are ±0.05 kK. Extinction coefficients are correct to within 5% based on triplicate analysis.

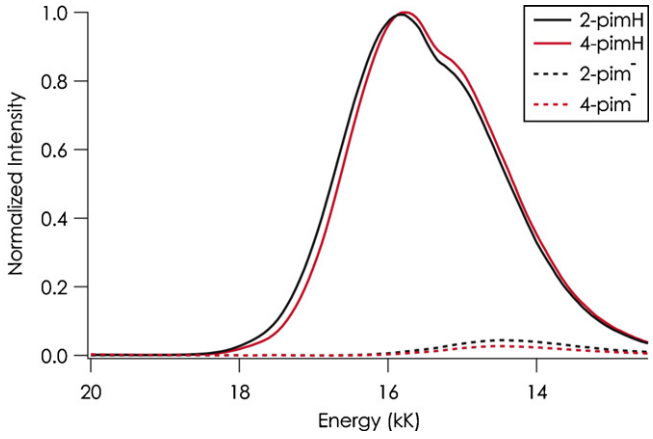

Fig. 7. Emission spectra of 10 μM $[Ru(bpy)_2(L)]^{2+}$ and $[Ru(bpy)_2(L)]^{+}$ (dotted lines) in degassed 5% methanol/water solution at room temperature. Excitation at 21.28 kK (21.05 kK long-pass filter). Spectral intensity corrected by λ^2_{nm} following conversion to energy units.

wave arises not from cathodic shifting of the $Ru^{III/II}$ potential but rather from a redox process occurring on the deprotonated pim^- ligand.

5. Excited state properties

Emission spectra in aqueous solution were obtained by 21.28 kK excitation of each of the 4 complexes (Fig. 7, Table 2). The protonated complexes exhibit intense emissions that upon deprotonation are red-shifted by ~1.3 kK and quenched 12-fold in **1** and 8-fold in **2**. The band shapes and positions of the protonated states of the complexes are slightly different, likely owing to differences in excited state structural perturbations. Energy differences between the $E_{0,0}$ and ν_{max} of the protonated complexes are not quantifiable within experimental error. Red-shifted emission spectra of the deprotonated complexes are likely attributable to increased π donation from the more electron-rich pim^- ligands. These shifts have been investigated by DFT calculations (*vide infra*).

Emission spectra also were recorded in deuterated solvent. In 5% CD_3OD/D_2O, the dedeuterated forms of **1** and **2** are quenched 14- and 13-fold relative to the deuterated complexes. Interestingly, both deuterated and dedeuterated states of **2** emit more strongly than those of **1**, suggesting a role for solvent and/or vibrational quenching of the complexes, likely at the distal amine the 4-pimH ligand.

Luminescence lifetime measurements were performed to probe the role of the non-coordinating imidazole nitrogen in deactivating the excited complexes (Table 3). In addition to decreased emission intensity, the lifetimes are considerably reduced upon deprotonation. While this behavior could be a consequence of the energy-gap law [43], we posit that it arises due to a change in character of the emissive state from ^{3}MLCT to ^{3}LLCT (*vide infra*). In protic solvent, **1** and **2** exhibit 7-fold increased emission decay rates upon deprotonation to $\mathbf{1}^-$ and $\mathbf{2}^-$. In deuterated solvent the lifetimes of both **1** and **2** increase in both protonation/deuteration states. Complex **2** exhibits longer lifetimes than **1** in all cases and presents a larger isotope effect (1.8 vs. 1.4). The observed isotope effects suggest that some combination of solvent hydrogen-bonding effects and N–H/D stretching contribute to excited state deactivation in these systems.

Table 2
Steady-state emission features[a] of $[Ru(bpy)_2(L)]^{2+}$.

L	5% MeOH:H_2O ν_{max} pH 3 (Φ_{em})	5% MeOH:H_2O ν_{max} pH 12 (Φ_{em})
2-pimH	15.82 (0.008)	14.49 (0.0003)
4-pimH	15.77 (0.013)	14.49 (0.0003)

[a] Emission energies are reported in kilokaisers. Quantum yields of emission (Φ_{em}) were calculated using $Ru(bpy)_3Cl_2$ as a standard.

Table 3
$[Ru(bpy)_2(L)]^{2+}$ luminescence lifetimes.[a].

Solvent	Lifetime (ns)			
	2-pimH	2-pim⁻	4-pimH	4-pim⁻
5% MeOH/H_2O	224	34	277	40
5% MeOD/D_2O	305	63	502	78

[a] Excitation at 21.46 kK (10 ns, pulsed Nd:YAG laser), emission detected at 15.38 kK, (protonated complexes) and 14.08 kK (deprotonated complexes), sample concentrations 10 μM, pH 3 for protonated and pH 12 for deprotonated complexes.

Radiative (k_r) and non-radiative (k_{nr}) rate constants for the protonated complexes in aqueous solutions were calculated from Eqs. (1) and (2):

$$\Phi = \varphi_{isc}\frac{k_r}{k_r + k_{nr}} = \varphi_{isc}k_r\tau_m \quad (1)$$

$$k_{nr} = \frac{1}{\tau_m} - k_r \quad (2)$$

where τ_m is the measured lifetime and φ_{isc} is the efficiency of intersystem crossing. Assuming $\varphi_{isc} = 1$ (all observed emission is phosphorescence), rate constants are: **1**, $k_r = 3.6 \times 10^4$ s^{-1}, $k_{nr} = 4.4 \times 10^6$ s^{-1}; **2**, $k_r = 4.7 \times 10^4$ s^{-1}, $k_{nr} = 3.6 \times 10^6$ s^{-1}. The faster non-radiative decay and decreased solvent isotope effect of **1** suggests a role for pimH-based non-radiative states that are populated with differing efficiencies between the two isomers. There is a similarity of this behavior to the divergent solvent isotope effects on the lifetimes of $[Ru(bpy)_3]^{2+}$ and $[Ru(phen)_3]^{2+}$ observed by Sriram and Hoffman [44], which were attributed to decay by differing relative amounts of non-radiative relaxation and upconversion to the triplet ligand field state. By analogy, quenching by upconversion appears to be more important relative to non-radiative relaxation in **1** than in $\mathbf{1}^-$, **2**, or $\mathbf{2}^-$.

6. Acid–base behavior

UV/vis monitored pH titrations reveal that **1** and **2** have strikingly differing acidities (pK_a of 7.9 ± 0.2 for **1**, 9.7 ± 0.2 for **2**). Spectroscopic and electrochemical parameters being approximately equal between the complexes, we suggest that the increased distance (calculated 4.14 Å for **1**, 4.27 Å for **2**, *vide infra*) between the acidic amine and the metal center of **2** is largely responsible for the decreased acidity of the molecule. Excited state pK_a values were approximated through use of the Förster cycle (**3**) [45], rather than the method of Sun and Hoffman [46], which requires pK_a measurements of the ground state of an oxidation state that mimics the

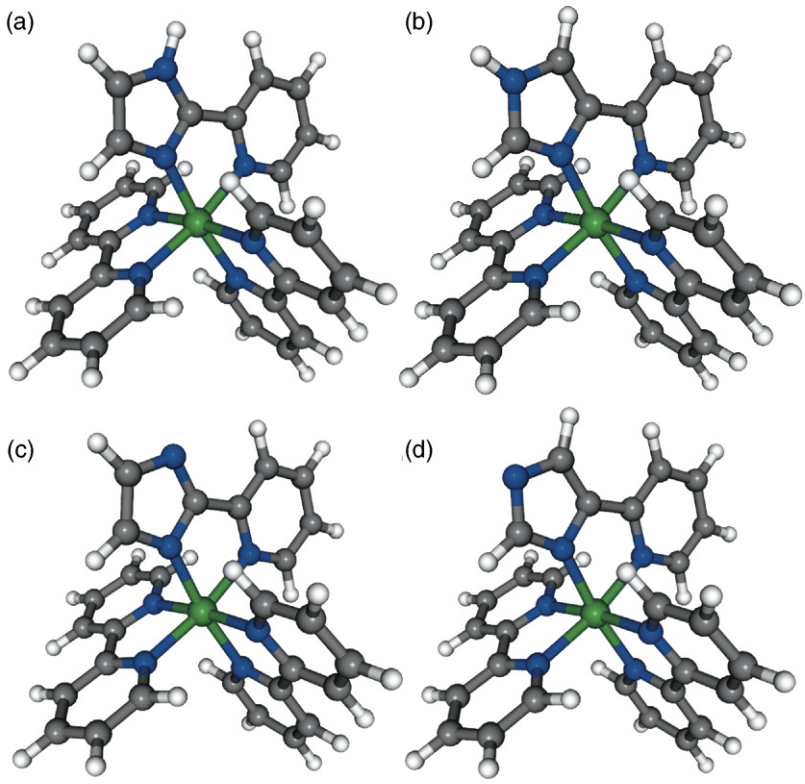

Fig. 8. Optimized gas-phase molecular structures of (a) **1**, (b) **2**, (c) $\mathbf{1}^-$, and (d) $\mathbf{2}^-$.

charge distribution of the excited state.

$$\Delta pK_a = pK_a - pK_a^* = \frac{E_{HA} - E_{A^-}}{2.3RT} \quad (3)$$

E_{HA} and E_{A^-} are the excited to ground state energy gaps ($E_{0,0}$) of the protonated and deprotonated complexes, respectively. R is the gas constant and T is the temperature (Kelvin). Estimation of $E_{0,0}$ as the initial rise of emission intensity results in approximately equivalent (~0.4 pK_a units) shifts towards greater acidity upon excitation. The photoacidic shift indicates that the long-lived emissive states of the molecules are bpy-rather than pimH-^{3}MLCT states. Population of pimH-based excited states, on the other hand, would transfer electron density to the non-coordinated amine, resulting in photobasicity, as observed with bipyrimidine and bipyrazine ligands (Table 4) [24,28,46]. These shifts in pK_a are substantial relative to the minor shifts in the case of **1** and **2**, as rather than tuning the acid–base properties by a coulombic interaction between the formally Ru^{III} and the imidazole, electron density is directly contributed to the ionizable nitrogen that stabilizes protonation. Similar behavior has been observed in the case of the non-coordinated imidazole in $Ru(bpy)_2(PhenImHPh)$ [18].

7. Theory

The application of DFT and time-dependent DFT (TDDFT) to the electronic structures of ground and excited states of transition metal complexes has been demonstrated as a valuable complement to experiment [50,51]. In the present case, calculations were performed using ORCA [52]. Molecular geometries were optimized in the gas phase (Fig. 8), with electronic structures subsequently calculated at these stationary points. The highest-occupied molecular orbital (HOMO) for both protonated molecules consists of a predominantly (~80% by Löwdin population analysis) Ru $4d_{z2}$ metal-centered (MC) orbital. The lowest unoccupied molecular orbital (LUMO) is a ligand-centered (LC) π^* orbital delocalized primarily over both bpy ligands. The computed gas-phase HOMO–LUMO gap calculated is 3.42 eV for both molecules. Modeling of solvation by water with COSMO [53] results in minor alterations to the electronic structures (Fig. 9). The HOMO–LUMO gaps shrink to 3.35 eV. pimH-based MOs exhibit the greatest perturbation upon inclusion of solvation into the calculations. There are minimal effects from solvation on the calculated molecular structures, as has been observed previously in calculations of the electronic structures of Ru(II) polyimine complexes [51].

Deprotonation leads to dramatic perturbation of the calculated ground-state electronic structure. The gas-phase HOMO–LUMO gaps shrink to 2.45 eV (**1**) and 2.61 eV (**2**). The HOMO of each molecule becomes a largely pim^--based M–L delocalized orbital. Thus, a ligand-centered redox locus may be implicated in the CVs of the deprotonated complexes (*vide supra*). The LUMO remains a bpy-centered ligand state, though with quite asymmetric population between the two bpy ligands. The metal-centered orbitals of $\mathbf{1}^-$ display larger energy gaps than those of $\mathbf{2}^-$, presumably owing to a stronger ligand field due to closer proximity of the distal $N^{\delta-}$ (calculated 4.16 Å for $\mathbf{1}^-$ vs. 4.31 Å for $\mathbf{2}^-$). The effect of COSMO modeled solvation is far more dramatic on the MO energies of the deprotonated complexes, likely due to charge localization on the deprotonated imidazole (Fig. 10). The HOMO–LUMO gaps increase to 3.01 eV (**1**) and 3.10 eV (**2**). This increase arises from greater

Table 4
Ruthenium diimine complex ground and excited state acidities.

Compound	pK_a	pK_a^*	Reference
1	7.9	7.5	This work
2	9.7	9.3	This work
$Ru(bpy)(bpz)_2^{2+}$	−0.72	3.5	[47]
$Ru(bpy)_2(bpm)^{2+}$	−2.9	1.95	[48]
$Ru(bpz)_3^{2+}$	−2.2	2.0	[28]
$Ru(bpm)_3^{2+}$	−1.0	2.2	[49]

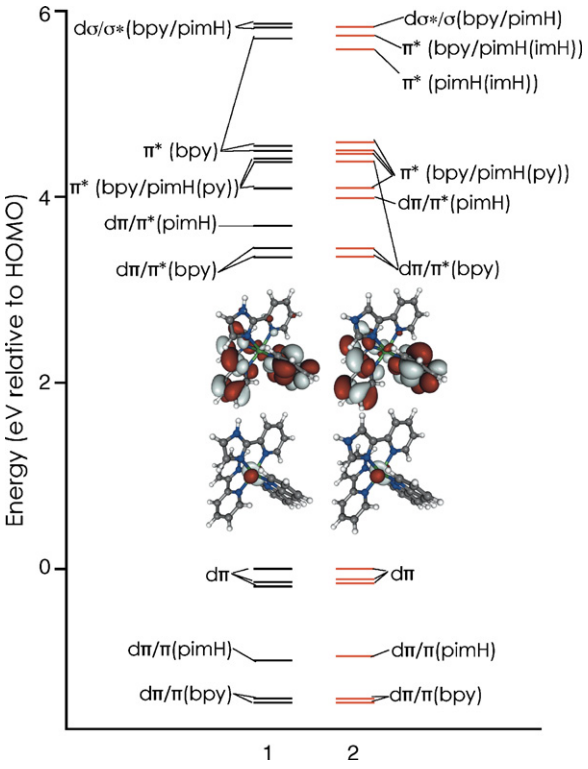

Fig. 9. Energy diagram for complexes **1** and **2** in solution (water, COSMO) with orbitals plotted on a scale normalized to the HOMO. Frontier orbital pictures are displayed.

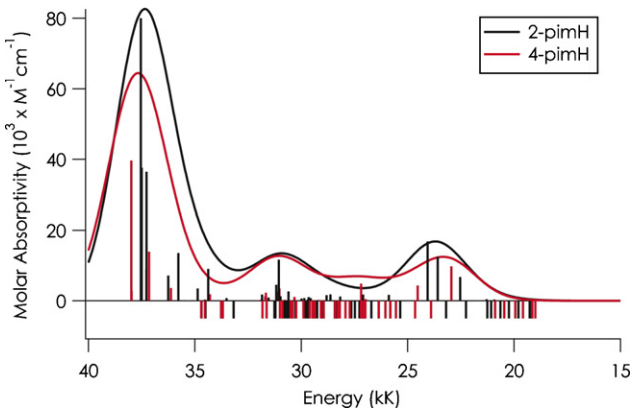

Fig. 11. TDDFT-calculated absorption spectrum of $Ru(bpy)_2L^{2+}$. Triplet excitations are plotted along the negative *y*-axis with arbitrary normalized intensity.

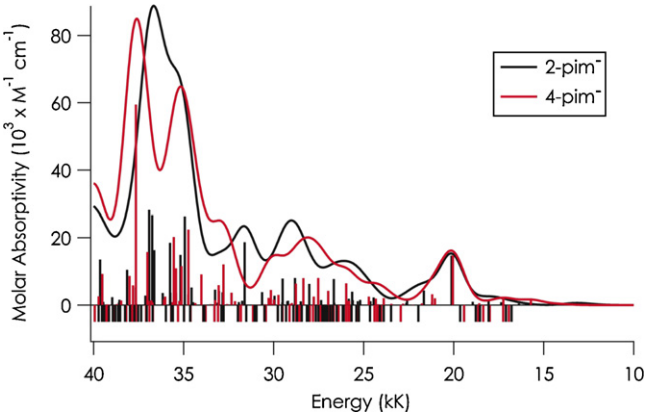

Fig. 12. TDDFT-calculated absorption spectrum of $Ru(bpy)_2L^{+}$ complexes. Triplet excitations are plotted along the negative *y*-axis with arbitrary normalized intensity.

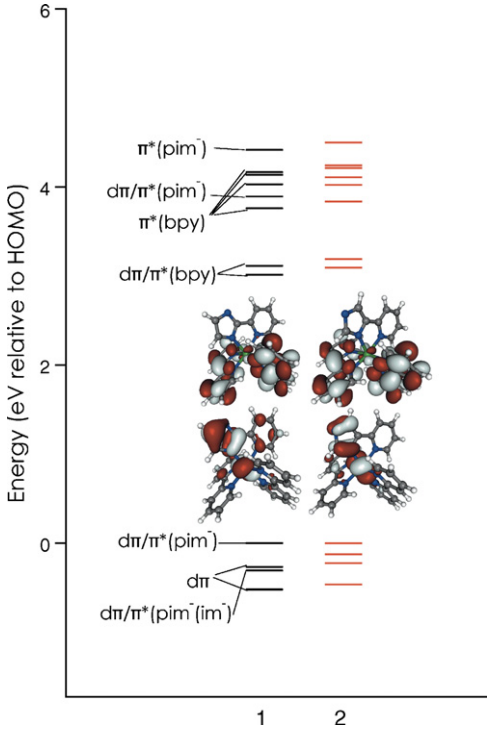

Fig. 10. Energy diagram of complexes $\mathbf{1}^-$ and $\mathbf{2}^-$ in solution (water, COSMO) with orbitals plotted on a scale normalized to the HOMO. Frontier orbital pictures are displayed.

destabilization of the LUMO relative to the HOMO upon inclusion of solvation.

From the optimized structures, TDDFT calculations were performed incorporating the COSMO solvation model with water chosen as the solvent (Fig. 11, Table 5). For simplicity, only singlet transitions were included in the spectra as triplet excitations can be expected to be minor contributors to the absorption spectra. Singlet energies and intensities accord with experiment. The calculations suggest that the broad absorption spectra are attributable to large numbers of ^{1}MLCT and ^{1}LLCT excited states. The spectrum of **1** arises from multi-component transitions; notably, many low-energy singlet and triplet excitations include contributions that are pimH-localized. Transitions in the spectrum of **1** arising purely from promotions to pimH-centered ^{1}LC states are conspicuously absent. However, pure pimH transitions are predicted for **2**; notably this transition gives rise to the intense absorption band at ~27 kK that is absent in the spectrum of **1**. Thus we suggest that the greater energy separations between pimH-based LC excited states and bpy-based LC excited states disfavor internal conversion to and subsequent pimH NH-based excited state deactivation of **2**, resulting in its longer emission lifetime.

The theoretical spectra of the deprotonated complexes are also in accord with experiment (Fig. 12). Almost double the number of singlet excited states are predicted between the intense, low energy 20 kK MLCT and the 40 kK LLCT system. As differences between excited state lifetimes measured for the deprotonated complexes are near the level of instrumental error, we have not made a thorough analysis of their calculated spectra in order to explain their relative photophysical properties.

Table 5
TDDFT-calculated singlet transitions for **1** and **2**.

1			
Transition energy[a]	Oscillator strength	Transition class[b]	Dominant transition orbitals
22.54	0.047	MLCT	dπ-bpy(π*), dπ-pimH(π*)
23.59	0.087	MLCT	dπ-bpy(π*), dπ-pimH(π*)
24.06	0.116	MLCT	dπ-bpy(π*), dπ-pimH(π*)
31.05	0.081	MLCT	dπ-bpy(π*)
34.37	0.063	LLCT	bpy(π)-pimH(π*), pimH(π)-pimH(π*)
35.77	0.094	LLCT	bpy(π)-pimH(π*), pimH(π)-pimH(π*)
37.54	0.553	LLCT	pimH(π)-bpy(π*), bpy(π)-bpy(π*)
2			
22.95	0.135	MLCT	dπ-bpy(π*)
24.53	0.060	MLCT	dπ-bpy(π*)
27.19	0.067	MLCT	dπ-pimH(π*)
31.03	0.048	MLCT	dπ-bpy/pimH(π*)
31.08	0.037	MLCT	dπ-bpy(π*)
37.99	0.548	LLCT	bpy(π)-pimH(π*), bpy(π)-bpy(π*)

[a] Transition energies in kK.
[b] Transitions are assigned in either the strict MLCT or LLCT limits; in many cases there is some orbital contribution from the metals that would technically classify the transitions as metal to metal/ligand charge transfers (MMLCT).

The lowest-lying triplet excited states of the protonated complexes accord with experiment; they are calculated as 19.16 kK for **1** and 19.00 kK for **2**. These excited states are entirely Ru 4d to bpy ^{3}MLCT in nature, consistent with the observed acid–base behavior. The lowest-lying triplet excited states of the deprotonated complexes also agree with experiment; these are calculated as 16.79 kK for $\mathbf{1}^-$ and 16.94 kK for $\mathbf{2}^-$. In this case the excited states are pimH to bpy ^{3}LLCT. Thus the energy-gap law cannot be applied as an explanation for the dramatically reduced quantum yields of the deprotonated complexes [54]. Rather, we suggest some combination of poor electronic coupling between the bpy and pimH ligands and efficient non-radiative deactivation by distal N^--solvent interactions as factors contributing to the weak emission.

8. Conclusions

The separations between the anodic and first cathodic electrochemical waves of **1** and **2** in both protonation states correlate with the lowest energy electronic absorption observed in each spectrum, as predicted by theory for redox processes with minimal reorganization [55]. The emission energies correlate with redox properties observed for other Ru-diimine complexes [15]. However, the observed photoacidity of Ru-pimH contrasts with the photobasicity observed for Ru(bpz) and Ru(bpm) by Meyer [24], Lever [28], and Hoffman [46], supporting the conclusion that the ^{3}MLCT excited states of 1 and 2 are bpy-centered. Complexes **1** and **2** display divergent acid–base and photophysical behaviors despite being largely indistinguishable spectroscopically and electrochemically. The former is attributable to the relative position of the acidic proton relative to the metal center and hence the electron localization in the ring [24]. The latter has been shown by DFT including TDDFT to arise from variable mixing of pimH-based MOs into singlet and triplet excited states, likely leading to the enhanced non-radiative decay observed for **1**. Due to the more sterically accessible N–H of 4-pimH relative to its well-studied isomer, along with the slower non-radiative relaxation of its ruthenium complexes, we suggest that molecules based on those reported herein could find potential use in studies of proton transfer and proton-coupled electron transfer. Tuning of photoacidities through substitutions on the bpy and pimH rings should be a straightforward means to synthesize a collection of Ru(II)-based photoacids.

9. Syntheses

All reagents were obtained from Sigma–Aldrich and used without further purification. Solvents for electronic absorption and emission measurements were of spectroscopic grade. $Ru(bpy)_2Cl_2$ (**6**) was prepared according to a published procedure [42].

2-(2′-pyridiyl)imidazole (2-pimH) (**7**) was prepared according to a published procedures [39].

4-tosyl-5-(2-pyridyl)oxazoline (8): Tosylmethyl isocyanide (0.975 g) was suspended in absolute ethanol. Pyridine-2-carboxaldehyde (0.5 mL) was added with stirring. Freshly crushed sodium cyanide (0.026 g) was added and the mixture was allowed to stir for 30 min. The product was filtered and washed with 20 mL of 1:1 ethyl ether:hexanes. The product was allowed to air-dry to give 1.219 g of an odorless tan powder, m.p. 121–124 °C. The proton NMR spectrum (300 MHz, $CDCl_3$, TMS reference) gave peaks at 2.458 ppm (s, 3H), 5.590 ppm (dd, 5.77, 1.65 Hz, 1H), 6.072 ppm (d, 5.63 Hz, 1H), 7.160 ppm (dd, 1.65, 0.41 Hz, 1H), 7.295 ppm (dd, 4.81, 1.24 Hz, 1H), 7.321 ppm (dd, 4.81, 1.09 Hz, 1H), 7.385 ppm (dd, 8.51, 0.69 Hz, 2H), 7.450 ppm (dm, 7.83 Hz, 1H), 7.759 ppm (td, 7.83, 1.79 Hz, 1H), 7.880 ppm (dm, 8.24 Hz, 2H), 8.645 ppm (ddd, 4.81, 1.65, 0.83 Hz, 1H). The proton decoupled ^{13}C NMR spectrum (75 MHz, $CDCl_3$, TMS reference) gave peaks at 22.001, 79.617, 90.559, 122.346, 124,346, 129.787, 130.080, 133.582, 137.445, 145.802, 150.479, 155.571, and 159.182 ppm.

4-(2′-pyridyl)imidazole (9): 8 (1.210 g) was dissolved in a resealable pressure tube with 40 mL of anhydrous ammonia-saturated methanol. The mixture was heated to 90–110 °C for 18 h and allowed to cool to room temperature. The solvent was removed by rotary evaporation and the remaining material was purified by chromatography on silica gel in 9:1 methylene chloride:hexanes to give 0.330 g of a dark brown oil with an odor of burnt butter. The oil was dissolved in isopropyl alcohol, acidified with hydrochloric acid, and precipitated as the dihydrochloride salt with acetone. The proton NMR spectrum (600 MHz, CD_3OD, solvent reference) gave peaks at 7.228 ppm (ddd, 7.37, 6.62, 1.72 Hz, 1H), 7.690 ppm (s, 1H), 7.784 ppm (d, 1.06 Hz, 1H), 7.807 ppm (td, 6.47, 0.89 Hz, 1H), 7.864 ppm (br d, 7.37 Hz, 1H), 8.472 ppm (br d, 6.32 Hz, 1H). The proton decoupled ^{13}C NMR spectrum (150 MHz, CD_3OD, solvent reference) gave peaks at 120.815, 123.205, 123.257, 137.759, 137.840, 150.026, 150.121, and 166.237 ppm.

$[Ru(bpy)_2(2\text{-pimH})](PF_6)_2$ (1): 0.520 g of **7** was combined with 0.145 g **4** and 0.040 g LiCl in 80 mL of a 3:1 absolute ethanol:water

mixture and heated at reflux for 4 h. A few drops of 37% HCl were added to effect complete isolation as the protonated complex. Ethanol was removed by rotary evaporation. 0.736 g of KPF_6 dissolved in a minimal amount of water was added to the red-orange solution to separate a dark red powder. The solid was filtered in a medium porosity frit and washed 3× each with 25 mL of water and 25 mL ethyl ether. The solid was dried by suction. The proton NMR spectrum (600 MHz, CD_2Cl_2, solvent reference) gave peaks at 6.471 ppm (s, 1H), 7.304 ppm (t, 7.20 Hz, 1H), 7.380 ppm (t, 7.20 Hz, 1H), 7.465 ppm (m, 4H), 7.539 ppm (d, 5.40 Hz, 1H), 7.724 ppm (d, 6.00 Hz, 1H), 7.793 ppm (d, 5.40 Hz, 2H), 7.839 ppm (d, 5.40 Hz, 1H), 8.007 ppm (dd, 8.4 Hz, 7.8 Hz, 2H), 8.050 ppm (t, 7.20 Hz, 3H), 8.270 ppm (d, 7.80 Hz, 1H), 8.367 ppm (t, 7.20 Hz, 2H), 8.414 ppm (t, 7.20 Hz 2H), 11.780 ppm (br, s, 1H). ESI MS *m*/*z* (calc) = 558.6 for $C_{28}H_{23}N_7Ru$; *m*/*z* (obs) = 558.3. Elemental analysis (single) (calc) C = 39.6, H = 2.70, N = 11.5, Ru = 11.91; (found) C = 39.86, H = 2.90, N = 11.52, Ru = 11.8.

[Ru(bpy)$_2$(4-pimH)](PF$_6$)$_2$·H$_2$O (2): Preparation of **2** proceeded the same as **1** using **9** as the ligand, though the material required additional purification. The red solid isolated following filtration of the PF_6 workup was applied to a silica gel column, washed with **1** column volume each of acetone, acetone containing 10% of a 10% saturated KNO_3 solution, and finally eluted with acetone containing 40% of a 10% saturated KNO_3 solution. Acetone was stripped by rotary evaporation from the pool of **2**, KPF_6 was added to crash out product. This material was collected on a fine porosity fritted glass funnel and washed with water and ether. The proton NMR spectrum (600 MHz, CD_2Cl_2, solvent reference) gave peaks at 7.205 ppm (t, 6.32 Hz, 1H), 7.275 ppm (s, 1H), 7.350 ppm (t, 6.53 Hz, 1H), 7.460 ppm (m, 3H), 7.493 ppm (t, 6.51 Hz, 1H), 7.707 ppm (d, 5.54 Hz, 1H), 7.804 ppm (d, 5.30 Hz, 1H), 7.876 ppm (m, 2H), 7.920 ppm (d, 7.87 Hz, 1H) 7.955 ppm (br s, 2H), 7.997 ppm (t, 7.82 Hz, 1H), 8.050 ppm (m, 3H), 8.345 ppm (d, 8.16 Hz, 1H), 8.375 ppm (d, 8.17 Hz, 1H), 8.415 ppm (d, 7.85 Hz, 2H), 11.192 ppm (br s, 1H). ESI MS *m*/*z* (calc) = 558.6 for $C_{28}H_{23}N_7Ru$; *m*/*z* (obs) = 558.3. Elemental analysis (single) (calc) C = 39.6, H = 2.70, N = 11.5, Ru = 11.91, loss on drying (H_2O) 2.07%; (found) C = 40.0, H = 3.04, N = 11.2, Ru = 11.77, loss on drying (H_2O) 2.07%.

10. Spectroscopic methods

Absorption spectra were recorded on a Hewlett Packard HP8453 diode array spectrophotometer. Samples for emission studies were prepared by 10× cycles of pump-purge with dry argon. Steady state emission spectra were recorded on a Jobin Yvon Spex Fluorolog-3-11. Sample excitation was achieved via a xenon arc lamp with a single monochromator providing wavelength selection. Right angle light emission was sorted using a single monochromator and fed into a Hammamatsu R928P photomultiplier tube with photon counting. Signal from scattered light was minimized using short and long pass filters where appropriate. Time-resolved measurements were conducted at the Beckman Institute Laser Resource Center. Laser excitation was achieved using 8 ns pulses at 355 nm from a Spectra-Physics Quanta-Ray Q-switched Nd:YAG laser (3rd harmonic) operating at 10 Hz to pump an optical parametric oscillator (OPO Spectra-Physics Quata-Ray MOPO-700) which was used to achieve laser pulses at 466 nm. Luminescence decays were detected using a Hamamatsu R928 PMT and recorded on a Tektronix model TDS-620A oscilloscope.

11. Electrochemical methods

CVs were measured using an edge-plane pyrolytic graphite electrode as the working electrode, platinum coil as the counter electrode, and a silver wire as a quasi-reference electrode. Ferrocene was added as an internal standard. Measurements were conducted under an argon atmosphere on 1 mM acetonitrile solutions containing 0.1 M tetrabutylammonium hexafluorophosphate as a supporting electrolyte. Measurements were made with a Model 660 Electrochemical Workstation (CH-Instrument, Austin).

12. Computational methods

DFT calculations including TDDFT were performed using the ORCA computational chemistry package [52]. Geometries were optimized for gas-phase molecules using the B3LYP hybrid functional with def2-TZV(P) [56] basis set. Relativistic effects were included using a zeroth-order approximation (ZORA) [57]. For TDDFT calculations, the conductor-like screening model (COSMO) [49] was included using dielectric parameters for water. For all calculations the RIJCOSX approximation [58–60] was employed with standard integration grids. Calculated absorption spectra were produced by summation of 3 kK full width at half maximum gaussians centered on the stick spectra with intensities proportional to oscillator strengths.

Acknowledgements

We thank Jay Winkler and Theis Brock-Nannestad for discussions. We thank Tony Vlček for a critical reading of this manuscript. We also thank John D. Roberts and Brian Stoltz for the kind loan of reagents and equipment. This work was supported by the NSF Center for Chemical Innovation (Powering the Planet, CHE-0802907 and CHE-0947829), the Arnold and Mabel Beckman Foundation, and CCSER (Gordon and Betty Moore Foundation).

References

[1] A.A. Vlček Jr., Coord. Chem. Rev. 200–202 (2000) 933.
[2] C.R. Bock, T.J. Meyer, D.G. Whitten, J. Am. Chem. Soc. 96 (1974) 4710.
[3] C. Creutz, N. Sutin, Inorg. Chem. 15 (1976) 496.
[4] O. Johansen, A. Launikonis, A.W.H. Mau, Aust. J. Chem. 33 (1980) 1643.
[5] J.J. Concepcion, J.W. Jurss, M.K. Brennaman, P.G. Hoertz, A.O.T. Patrocinio, N.Y.M. Iha, J.L. Templeton, T.J. Meyer, Acc. Chem. Res. 42 (2009) 1954.
[6] W.J. Eilbeck, F. Holmes, G.G. Phillips, A.E. Underhill, J. Chem. Soc. A (1967) 1161.
[7] W.J. Eilbeck, F. Holmes, J. Chem. Soc. A (1967) 1777.
[8] W.J. Eilbeck, F. Holmes, G. Phillips, J. Chem. Soc. A (1970) 689.
[9] F. Holmes, K.M. Jones, E.G. Torrible, J. Chem. Soc. (1961) 4790.
[10] B. Chiswell, F. Lions, B.S. Morris, Inorg. Chem. 3 (1964) 110.
[11] R.K. Boggess, R.B. Martin, Inorg. Chem. 13 (1974) 1525.
[12] M. Haga, Inorg. Chim. Acta 75 (1983) 29.
[13] M. Haga, A. Tsunemitsu, Inorg. Chim. Acta 164 (1989) 137.
[14] J.G.D.M. Atton, R.D. Gillard, Transition Met. Chem. 6 (1981) 351.
[15] G. Orellana, M.L. Quiroga, A.M. Braun, Helv. Chim. Acta 70 (1987) 2073.
[16] G. Orellana, C. Alvarez-Ibarra, M.L. Quiroga, Bull. Soc. Chim. Belg. 97 (1988) 731.
[17] G. Stupka, L. Gremaud, A.E. Williams, Helv. Chim. Acta 88 (2005) 487.
[18] A. Quaranta, F. Lachaud, C. Herrero, R. Guillot, M.-F. Charlot, W. Leibl, A. Aukauloo, Chem. Eur. J. 13 (2007) 8201.
[19] X.-J. Yang, F. Drepper, B. Wu, W.-H. Sun, W. Haehnel, C. Janiak, Dalton Trans. (2005) 256.
[20] K. Pachhunga, B. Therrien, K.A. Kreisel, G.P.A. Yap, M.R. Kollipara, Polyhedron 26 (2007) 3638.
[21] H. Mishra, R.J. Mukherjee, Organomet. Chem. 691 (2006) 3545.
[22] A. Wu, J. Masland, R.D. Swartz, W. Kaminsky, J.M. Mayer, Inorg. Chem. 46 (2007) 11190.
[23] J.T. Fletcher, B.J. Bumgarner, N.D. Engels, D.A. Skoglund, Organometallics 27 (2008) 5430.
[24] D.P. Rillema, G. Allen, T.J. Meyer, D. Conrad, Inorg. Chem. 22 (1983) 1617.
[25] Z. Chen, J.J. Concepcion, J.W. Jurss, T.J. Meyer, J. Am. Chem. Soc. 131 (2009) 15580.
[26] P. Ford, de F.P. Rudd, R. Gaunder, H. Taube, J. Am. Chem. Soc. 90 (1968) 1187.
[27] A. Albert, P.J. Taylor, J. Chem. Soc. Perkin Trans. II (1989) 1903.
[28] R.J. Crutchley, N. Kress, A.B.P. Lever, J. Am. Chem. Soc. 105 (1983) 1170.
[29] G. Yagil, Tetrahedron 23 (1967) 2855.
[30] P.J. Morris, R.B. Martin, J. Am. Chem. Soc. 92 (1970) 1543.
[31] M.H.V. Huynh, T.J. Meyer, Chem. Rev. 107 (2007) 5004.
[32] J.M. Mayer, Annu. Rev. Phys. Chem. 55 (2004) 363.
[33] J. Rosenthal, D.G. Nocera, Acc. Chem. Res. 40 (2007) 543.
[34] A. Wu, J.M. Mayer, J. Am. Chem. Soc. 130 (2008) 14745.
[35] J.R. Bryant, J.M. Mayer, J. Am. Chem. Soc. 125 (2003) 10351.
[36] J.L. Cape, M.K. Bowman, D.M. Kramer, J. Am. Chem. Soc. 127 (2005) 4208.

[37] M.K. Ludlow, A.V. Soudackov, S. Hammes-Schiffer, J. Am. Chem. Soc. 131 (2009) 7094.
[38] B. Radziszewski, Chem. Ber. 15 (1882) 2706.
[39] T.I.A. Gerber, E. Hosten, P. Mayer, Z.R. Tshentu, J. Coord. Chem. 59 (2006) 243.
[40] G.R. Clemo, T. Holmes, G.C. Leith, J. Chem. Soc. (1938) 753.
[41] F. Wang, A.W. Schwabacher, Tetrahedron Lett. 40 (1999) 4779.
[42] B.P. Sullivan, D.J. Salmon, T.J. Meyer, Inorg. Chem. 17 (1978) 3334.
[43] J.R. Lakowicz, Principles of Fluorescence Spectroscopy, 3rd ed., Springer, New York, 2006.
[44] R. Sriram, M.Z. Hoffman, Chem. Phys. Lett. 85 (1982) 572.
[45] T.H. Förster, Z. Electrochem. 54 (1950) 42.
[46] H. Sun, M.Z. Hoffman, J. Phys. Chem. 97 (1993) 5014.
[47] K.A. Goldsby, T.J. Meyer, Inorg. Chem. 23 (1984) 3002.
[48] Md.K. Nazeeruddin, K. Kalyanasundaram, Inorg. Chem. 28 (1989) 4251.
[49] M. Hunziker, A. Ludi, J. Am. Chem. Soc. 99 (1977) 7370.
[50] A.A. Vlček Jr., S. Zális, Coord. Chem. Rev. 251 (2007) 258.
[51] E. Jakubikova, W. Chen, D.M. Dattelbaum, F.N. Rein, R.C. Rocha, R.L. Martin, E.R. Batista, Inorg. Chem. 48 (2009) 10720.
[52] F. Neese, U. Becker, D. Ganyushin, A. Hansen, D.G. Liakos, C. Kollmar, S. Kossmann, T. Petrenko, C. Reimann, C. Riplinger, K. Sivalingam, E. Valeev, B. Wezisla, F. Wennmohs, ORCA, version 2.7.0b, University of Bonn, Bonn.
[53] A. Klamt, G.J. Schüürmann, Chem. Soc. Perkin Trans. 2 (1993) 799.
[54] D.J. Stufkens, A.A. Vlček Jr., Coord. Chem. Rev. 177 (1998) 127.
[55] A.A. Vlček, Electrochim. Acta 13 (1968) 1063.
[56] D.A. Pantazis, X.Y. Chen, C.R. Landis, F. Neese, J. Chem. Theory Comput. 4 (2008) 908.
[57] C. van Wuellen, J. Chem. Phys. 109 (1998) 392.
[58] F. Neese, F. Wennmohs, A. Hansen, U. Becker, Chem. Phys. 356 (2009) 98.
[59] S. Kossman, F. Neese, Chem. Phys. Lett. 481 (2009) 240.
[60] F. Neese, J. Comput. Chem. 24 (2003) 1740.